# Graphene Drape Minimizes the Pinning and Hysteresis of Water Drops on Nanotextured Rough Surfaces

Eklavya Singh,[†,§] Abhay V. Thomas,[†,§] Rahul Mukherjee,[†] Xi Mi,[‡] Farzad Houshmand,[†] Yoav Peles,[†] Yunfeng Shi,[‡] and Nikhil Koratkar[†,‡,*]

[†]Department of Mechanical, Aerospace, and Nuclear Engineering and [‡]Department of Materials Science and Engineering, Rensselaer Polytechnic Institute, Troy, New York 12180, United States. [§]E.S. and A.V. T. contributed equally to this work.

ABSTRACT Previous studies of the interaction of water with graphene-coated surfaces have been limited to flat (smooth) surfaces. Here we created a rough surface by nano-patterning and then draped the surface with a single-layer graphene sheet. We found that the ultrasheer graphene drape prevents the penetration of water into the textured surface thereby drastically reducing the contact angle hysteresis (which is a measure of frictional energy dissipation) and preventing the liquid contact line from getting pinned to the
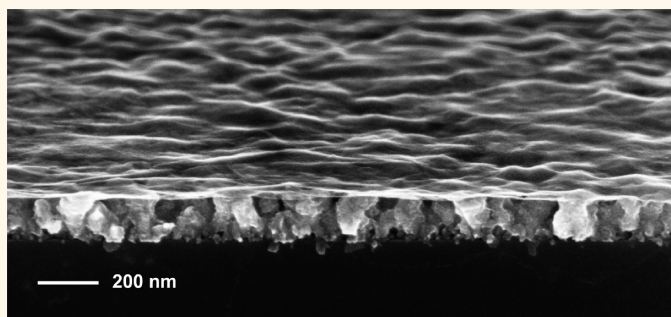
substrate. This has important technological implications since the main obstacle to the motion of liquid drops on rough surfaces is contact angle hysteresis and contact line pinning. Graphene drapes could therefore enable enhanced droplet mobility which is required in a wide range of applications in micro and nanofluidics. Compared to polymer coatings that could fill the cavities between the nano/micropores or significantly alter the roughness profile of the substrate, graphene provides the thinnest (*i.e.*, most sheer) and most conformal drape that is imaginable. Despite its extreme thinness, the graphene drape is mechanically robust, chemically stable, and offers high flexibility and resilience which can enable it to reliably drape arbitrarily complex surface topologies. Graphene drapes may therefore provide a hitherto unavailable ability to tailor the dynamic wettability of surfaces for a variety of applications.

KEYWORDS: graphene drape · contact angle hysteresis · contact line pinning · energy dissipation · droplet mobility

The motion of water drops on solid surfaces is required in many applications including lab-on-chip devices, biomedical applications, high throughput assays, surfaces for dropwise condensation, water harvesting, low-friction coatings, and self-cleaning and antifouling surfaces.[1−7] The key to successfully moving water drops on surfaces is to reduce the adhesion of water with the surface. This can be achieved by tailoring the chemistry of the surface or its roughness.[8−11] Many studies have utilized microscale or nanoscale surface roughness features to entrap air pockets underneath the water droplet.[12−15] Under static conditions such surface roughness features are effective in supporting the water drop in a suspended (Cassie[16]) state which results in weak surface adhesion. However under dynamic conditions (*e.g.*, droplet motion or impact), water drops can possess sufficient kinetic energy to penetrate into these roughness features and force out the entrapped air; this is called the Wenzel State.[17] Such Cassie-to-Wenzel state transition pins the drop to the surface and generates large differences between the advancing and receding water contact angles (contact angle hysteresis), which is a measure of the friction at the droplet−substrate interface. Here we show using both experiments and modeling that droplet pinning and contact angle hysteresis on rough surfaces can be dramatically reduced by draping an ultrathin and flexible mono-layer graphene sheet over the surface. This has important implications for the design of ultrathin and minimally invasive coating materials that enhance droplet mobility on textured (rough) surfaces.

(a)

(b)

(c)

(d)
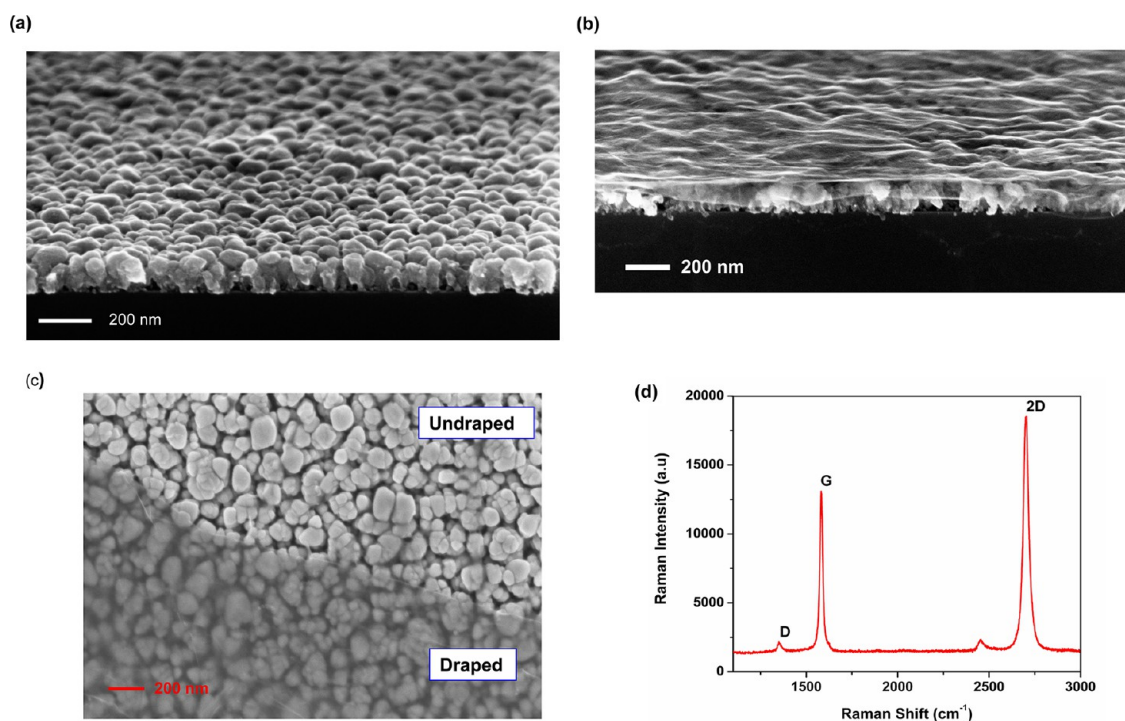
Figure 1. Characterization of the Cu nanorods surface with and without the graphene drape. (a) Scanning electron micrograph (SEM) of the aligned array of Cu nanorods deposited on a flat Si wafer by oblique angle sputter deposition. (b) Corresponding image of the same Cu nanorods surface after it has been draped by a single-layer graphene sheet. (c) Top view SEM image of the Cu nanorods surface. The darkened region represents the portion of the array that is draped while the lighter region is the undraped portion. (d) Typical Raman spectra of the graphene drape showing the Raman G ($\sim$1584 cm^{-1}) and 2D ($\sim$2685 cm^{-1}) band peaks that are characteristic of monolayer graphene. Note the strongly suppressed defect related D peak ($\sim$1350 cm^{-1}) which indicates high quality graphene.

RESULTS AND DISCUSSION

Experiments. The nanotextured (rough) surface in our study comprises an aligned array of Copper (Cu) nanorods (Figure 1a) that are deposited on a flat silicon wafer using oblique angle sputter deposition (Materials and Methods).[18,19] The average height of the Cu nanorods is $\sim$200 nm, with a maximum diameter of $\sim$50 nm (at the fanned out section at the top) and a minimum diameter of $\sim$20 nm (at the base). The average wall-to-wall spacing between the Cu nanorods is $\sim$30 nm (Figure 1c). The water contact angle for the Cu nanorods surface can be predicted by using the well-established Cassie and Baxter equation.[16] $\cos\theta_c = f(\cos\theta_o + 1) - 1$, where θ_o is the contact angle on a flat Cu surface, θ_c is the apparent contact angle and f is the porosity, expressed as the projected area of the solid—liquid contacts divided by the total projected area of the droplet. On the basis of the image analysis from SEM observations (Figure 1c), the porosity, $f = 0.54$. The water contact angle measured on a flat Cu film (θ_o) deposited under the same conditions as the Cu nanorods was $\sim$86°. Note that a pristine (perfectly clean) Cu surface should show zero water contact angle[20] but in practice formation of passivation layers[21] (typically CuO and Cu$_2$O) result in larger contact angles. By substituting $\theta_o = 86°$ for Cu, we get a predicted water contact angle, θ_c of 115.24° for the Cu nanorods array, which shows good agreement with

the experimental static water contact angle value which was $\sim$114 $\pm$ 2 degrees. This confirms that when water droplets are gently released on the surface of the Cu nanorods array, they lie in the suspended Cassie state due to the entrapped air pockets formed within the porous Cu nanorod network.

Next, we draped the Cu nanorods surface with a monolayer graphene sheet as indicated in Figure 1b. We synthesized monolayer graphene by chemical vapor deposition (CVD) on Cu foils using methane[22] as the feedstock (Materials and Methods). After growth, a thin poly(methyl—methacrylate) (PMMA) film was coated on the graphene/Cu substrate. The Cu substrate was etched in dilute ammonium persulfate (0.25 M), and the graphene/PMMA film was transferred onto the Cu nanorods array (see Materials and Methods for precautions taken to achieve a clean and crackless transfer). After the transfer, the PMMA was dissolved away using acetone. The scanning electron microscopy (SEM) image in Figure 1b shows a typical image of the Cu nanorods surface draped with a monolayer graphene sheet. The graphene drape uniformly covers the entire surface and there is no indication of any cracks or tears in the drape. The extreme thinness and flexibility of the drape also enables it to conform to the surface topology of the Cu nanorod tips. A typical top view SEM image of the graphene

draped Cu nanorods surface is shown in Figure 1c. The contrast between the portion of the surface that is draped by the monolayer graphene and the part which lies exposed is evident. To confirm that the graphene that we are using is monolayer, we used Raman spectroscopy (Materials and Methods) to measure the characteristic Raman G, and 2D bands (Figure 1d). The ratio of the integrated intensity of the Raman G and 2D peaks ($\sim$0.4), the position of the 2D peak at $\sim$2685 cm^{-1}, and the full width at half-maximum ($\sim$32 cm^{-1}) of the 2D peak are all consistent with the literature[22,23] for single-layer graphene grown by chemical vapor deposition on Cu foils.

Advancing and receding water contact angle measurements were performed using a 500-F4 Rame-Hart goniometer for images and the low-bond axisymmetric drop shape analysis technique was used to determine the contact angles (Materials and Methods). In the experiments a $\sim$1 μL volume water drop was brought in contact with the surface and subsequently the volume of the drop was increased and then decreased to advance and retract the liquid front. This was repeated several times to check the reproducibility of the results. Figure 2a shows the advancing and receding conditions created by dispensing and retracting water at a rate of $\sim$0.40 μL/s for the Cu nanorods surface with and without a monolayer graphene drape. It is evident that the graphene drape has a "dramatic" influence on the receding liquid front. Without the drape the liquid front gets strongly pinned to the solid surface which lowers the receding water contact angle to nearly zero degrees. By contrast with the drape, the water drop is no longer pinned and is able to retract freely on the surface (Figure 2a).

Additional measurements were performed by varying the number of graphene layers on the surface. For this multiple transfers were carried out to deposit bilayer and then trilayer graphene drapes on the Cu nanorods surface. The effect of the number of graphene layers in the drape on the advancing/receding contact angles is shown in Figure 2b. The advancing contact angle of the baseline Cu nanorods surface (without the drape) is $\sim$120°, while its receding contact angle is nearly zero degrees. With the monolayer graphene drape, the advancing water contact angle drops to $\sim$102°. This shows that on such strongly hydrophobic surfaces, even a single graphene layer fails to exhibit the wetting transparency effect that has been reported on flat surfaces at lower contact angles.[23] This deviation from wetting transparency has been explained by Strano, Blankschtein, and co-workers[24] who showed that the water contact angle on an isolated monolayer graphene sheet is $\sim$96°. Consequently, the maximum contact angle that can be achieved on any graphene-draped surface (including the Cu nanorods surface) will be limited to $\sim$96° provided that the graphene sheet remains relatively

flat and does not droop (or sag) into the interstices between the roughness features (Supporting Information, Figure S1). Since the advancing contact angle is typically several degrees greater than the static value, the $\sim$102° advancing contact angle measured on the graphene-draped Cu nanorods surface is therefore consistent with the $\sim$96° static contact angle predicted in ref 24. However the key observation from Figure 2b is that graphene draping results in a large increase in the receding water contact angle from nearly 0 degrees to $\sim$60°. With increasing number of graphene layers in the drape (i.e., for bilayer and trilayer coatings) the advancing contact angle remains fairly constant at $\sim$100°, while the receding contact angle continues to increase to $\sim$70° for bilayer graphene and $\sim$80° for the trilayer graphene drape. In Figure 2c, we have plotted the contact angle hysteresis (which is the difference between the advancing and receding contact angles) vs the number of graphene layers in the drape. The contact angle hysteresis falls sharply from $\sim$120° for the baseline Cu nanorods surface to $\sim$45° for the monolayer graphene drape and then continues to decrease with increasing number of graphene layers in the drape. For the trilayer graphene drape, the contact angle hysteresis reduces to $\sim$25°.

The very high contact angle hysteresis observed for the baseline Cu nanorods surface is caused by a Cassie-to-Wenzel state transition which occurs when the volume of the liquid drop is being increased (i.e., during the advancing phase). This can be understood by considering the critical pressure (P_c) required to transition the water drop from the Cassie to the Wenzel state: $P_c = (-\gamma \cos(\theta_o) \times L)/A$.[25] Here γ is the surface tension of water, L is the perimeter of the nanopore formed between the Cu nanorods, A is the cross sectional area of the nanopore and θ_o is the water contact angle of the pore walls ($\sim$86° for Cu). Since $\theta_o < 90$° (i.e., $\cos(\theta_o) > 0$), the critical pressure is negative which implies that the Cassie state is inherently unstable, and therefore even a slight disturbance to the liquid drop (during the advancing phase) will cause the water to penetrate into the pores formed between the Cu nanorods. The result of this is that the entrapped air pockets formed in the nanotextured surface are expelled and the liquid drop now resides in the sticky Wenzel state. The droplet contact line is therefore strongly pinned to the surface and when the drop is retracted the receding contact angle remains close to zero to ensure that the contact length between the water drop and the substrate remains essentially unchanged.

Draping the Cu nanorods surface with a minimally invasive (ultrasheer) but impermeable[26] graphene sheet appears to prevent water penetration into the nanopores in the Cu nanorods surface. Consequently the liquid drop remains suspended on the top of the graphene-draped Cu nanorods surface which prevents
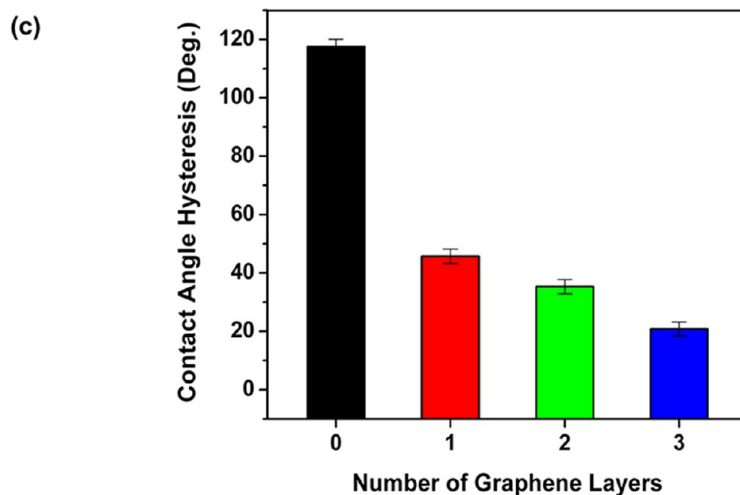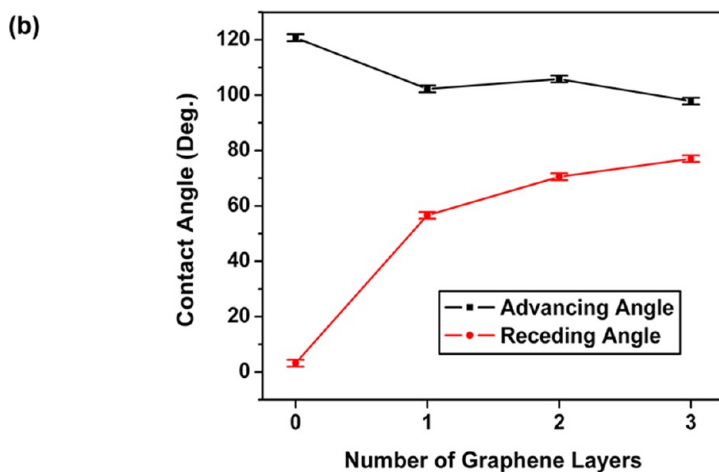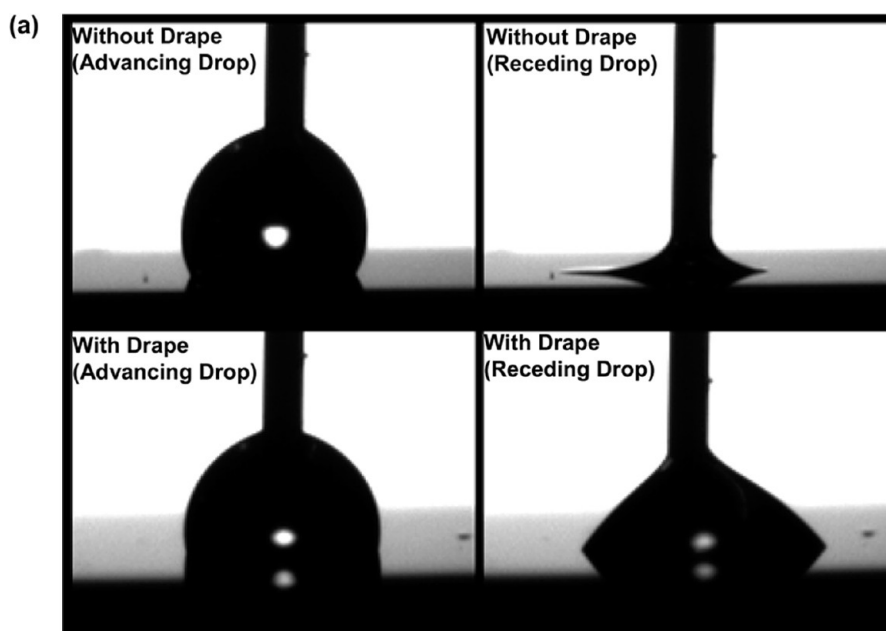
Figure 2. Contact angle hysteresis measurements. (a) Images of advancing and receding water drops on the Cu nanorods surface with and without the graphene drape. (b) Advancing and receding water contact angles of the drop plotted *vs* the number of graphene layers in the drape. (c) Measured contact angle hysteresis plotted *vs* the number of graphene layers in the drape.

(a)

(b)
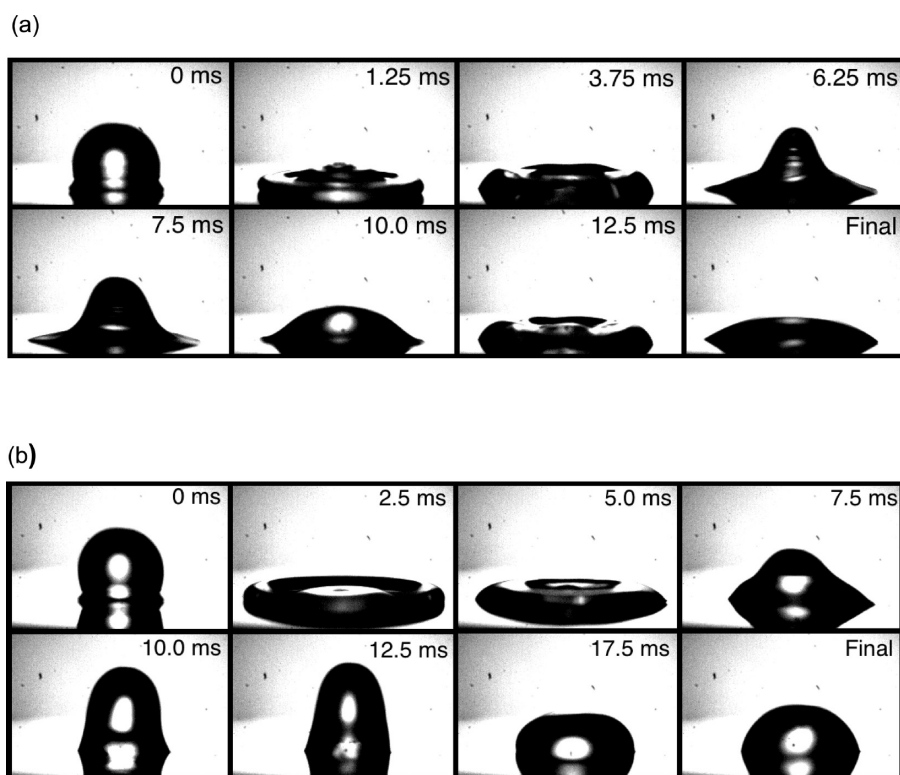
Figure 3. Droplet impact experiments. (a) Snapshots of a water droplet impacting the baseline Cu nanorods surface at a velocity of ~60 cm/sec. The droplet spreads into a pancake shape as its kinetic energy is converted into elastic strain energy in the drop; however, during the receding phase, the water contact line gets strongly pinned to the substrate, which results in large contact angle hysteresis. **(b)** Corresponding real-time snapshots of a similar sized water droplet striking the surface of the graphene draped Cu nanorods surface at a velocity of ~60 cm/sec. In this case the droplet contact line does not get pinned to the surface and extends/contacts periodically as the droplet repeatedly advances and then recedes on the graphene-draped surface.

the contact line from getting pinned to the substrate roughness features (this increases the receding contact angle by ~60° compared to the undraped surface). With increasing number of graphene layers in the drape, the receding water contact angle continues to increase and the contact angle hysteresis decreases further as shown in Figures 2b,c. This could be an artifact of the greater degree of smoothening of the Cu nanorods surface with increasing number of graphene layers in the drape. To study this we used atomic force microscopy (AFM) imaging to measure the rms roughness for the 1-layer, 2-layer, and 3-layer drapes. However we found that there was no significant change in the rms roughness values as a function of the number of graphene layers in the drape. In addition to roughness, contact angle hysteresis also depends on defects on the surface which can pin the water contact line. When we transfer the first graphene layer, damage (*e.g.*, nanometer size holes or cracks) could be more easily induced since the graphene sheet comes in direct contact with the sharp Cu nanorod tips. Subsequent layers of graphene that are transferred onto the surface are expected to be relatively less defective due to the cushioning effect of the underlying sheets. It was challenging to quantify the defect density of graphene from Raman after it has been transferred onto the Cu

nanorods surface because the background signal from the Cu nanorods interferes strongly with the graphene Raman signature. It should be noted that increasing the number of graphene layers will also enhance the ability of the drape to prevent water penetration into the interstices formed between the Cu nanorods. Quantitative measurement of the defectiveness of the drape as the number of graphene layers is increased is an important issue and warrants further investigation.

Droplet impact tests were also performed to evaluate the ability of the graphene drape to prevent Cassie-to-Wenzel state transition under impact conditions. Droplets as large as $1-2$ mL were dropped on the samples from a fixed height using a microsyringe to impact the surface at velocities ranging from 50 to 70 cm/sec. A high-speed camera (PhantomV4) operated at 800 frames per second with ~80 μs exposure time was used in this study. Time lapse images for the relevant advancing and receding stages of the droplets are shown in Figure 3 at an impact velocity of ~60 cm/sec. For the baseline (*i.e.*, undraped) Cu nanorods surface (Figure 3a), the droplet first deforms and flattens into a pancake shape (this is the advancing phase). However during the retraction phase the droplet gets strongly pinned to the substrate. This is

(a)

(b)
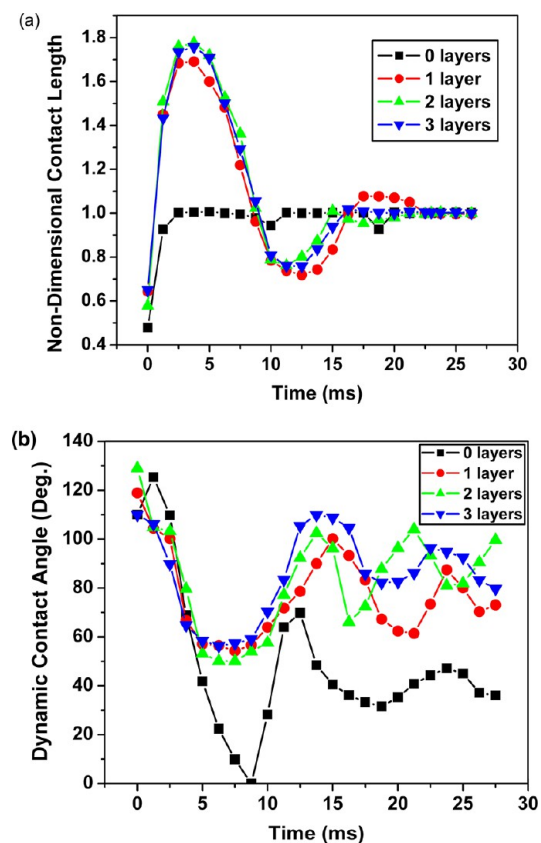
Figure 4. Nondimensional drop contact length and dynamic contact angle during droplet impact. (a) Nondimensional contact length (defined as the real-time contact length at the drop/substrate interface normalized by the final equilibrium contact length) plotted *vs* time after impact. (b) Dynamic water contact angle (obtained by averaging the instantaneous, real-time contact angles on the left and right contact lines of the droplet) plotted *vs* the time after impact.

evident in Figure 4a where we plot the real-time contact length of the droplet normalized by the equilibrium contact length of the same drop. The equilibrium contact length is measured after the drop is no longer in motion and has fully settled on the solid surface. Figure 4a indicates that without the drape the droplet expands to a maximum size (normalized contact length = 1.0) which occurs at ~1.25 ms (which is the end of the advancing phase), but then at subsequent times the nondimensional contact length remains fixed at ~1.0 and does not reduce which confirms that the droplet is now pinned. By contrast on the Cu nanorods surface with the monolayer graphene drape (Figure 3b) the droplet spreads into a pancake shape but then retracts fully (see time = 12.5 ms in Figure 3b) and does not get pinned to the substrate. In fact the contact line continues to advance and retract for several cycles as indicated by the sinusoidal fluctuations in the nondimensional contact length of the drop (Figure 4a); these oscillations persist for over 25 ms as opposed to ~1.25 ms for the baseline (undraped) Cu nanorods surface.

The droplet impact phenomenon was studied in further detail by plotting the dynamic contact angle against time as shown in Figure 4b. For the baseline Cu nanorods surface the dynamic contact angle decreases rapidly from ~120° during the short-lived advancing phase to 0 degrees during the retraction of the drop. Subsequently the dynamic contact angle fluctuates as the pinned drop pulsates on the surface (Supporting Information, Video S1) and settles to a value of ~40°. When the surface is draped with graphene, the initial dynamic contact angle is again ~120°, but this time the water contact angle never drops below ~60° even during the retraction phase and continues to oscillate for a prolonged time period as the droplet vibrates freely (no pinning) on the graphene draped surface (Supporting Information, Video S2). We fitted the results for the dynamic contact angle shown in Figure 4b to an exponentially decaying sinusoidal function expressed as: $e^{-\zeta \omega t} A \sin(\omega t)$, where ζ is the damping ratio which quantifies the energy dissipation, ω is the oscillation frequency, t is time, and A is the initial amplitude of the contact angle fluctuation. The measured damping ratio (ζ) of the bare Cu nanorods surface was ~0.164 which reduces to ~0.034 when a monolayer graphene drape is placed over the surface. This indicates that the energy dissipation is ~382% greater when the water droplet is impacted on the baseline Cu nanorods surface as compared to the corresponding graphene draped surface. Note that the decay in the oscillation amplitude of the dynamic contact angle (as in Figure 4b) reflects the energy dissipated at the interface as well as in the bulk liquid droplet. To focus more narrowly on the liquid−solid interface, we investigated the damping ratio measured with respect to the oscillations in the nondimensional contact length. From the time traces in Figure 4a, we conclude that the Cu nanorods surface is overdamped ($\zeta \geq 1$, since no oscillations were observed), while the graphene draped surface gave a damping ratio (ζ) of ~0.072. Therefore for the liquid−solid interface, the graphene-draped surface exhibits over an order of magnitude less frictional energy dissipation as compared to the baseline Cu nanorods surface.

Molecular Dynamics Simulations. To better understand and interpret the experimental observations, we conducted molecular dynamics (MD) simulations to compute both the advancing and receding contact angles for a water droplet on a model nanotextured substrate with and without graphene draping. As a full MD simulation with the actual Cu nanorod dimensions (~200 nm in height and ~50 nm in diameter) is beyond the current computational capability, we chose a rough Cu surface (with steps that are 1.5 nm long, 0.6 nm high, repeating with a periodicity of 3.0 nm) as the model nanotextured substrate. To model the actual experimental Cu nanorods surface,

the simulation system would have to be at least a few micrometers to be representative. To our knowledge, micrometer-sized system with long-range interaction (water–water interaction contains long-range Coulombic interaction) is still out of reach for full MD simulations.

We setup the system in the following way. The size of the simulation box is $307.68 \times 22.20 \times 200$ Å^3. This simulation box is designed to be thin-slab-like in the y-direction in order to avoid size-dependent contact angle due to line tension.[23] Three-layered thick square-wave-shaped features are constructed on top of the nine-layered Cu(111) slab. The graphene draping is placed at 2.8 Å away on top of the Cu substrate. The substrate (Cu and graphene) is kept rigid throughout the simulation. It has been shown that the water contact angle is almost identical on either rigid or flexible substrates.[28] There were 4000 water molecules initially packed orderly on top of the substrate and then relaxed under constant temperature to form the droplet. We used the SPC/E model[29] with slight modification for water–water interactions, which consists of Coulombic interactions between partial charges on O ($-0.8476e$) and H ($+0.4238e$) atoms, and an O–O Lennard-Jones (LJ) interaction with $\varepsilon_{O-O} = 0.6502$ kJ/mol, $\sigma_{O-O} = 3.166$ Å and a cutoff of 10 Å. Harmonic bond and angle constraints are used to keep the O–H distance close to 1 Å and the H–O–H angle close to 109.47. LJ potentials are used for both C–O and Cu–O interactions. The LJ parameters are determined as $\varepsilon_{C-O} = 0.3975$ kJ/mol, $\sigma_{C-O} = 3.19$ Å, $\varepsilon_{Cu-O} = 0.7113$ kJ/mol and $\sigma_{C-O} = 3.19$ Å to match the experimental contact angles for water/graphite and water/Cu.

The system was equilibrated at 298 K for 2.4 ns to reach equilibrium under an NVT ensemble with an integration step of 1 fs. We monitored the potential energy, which reaches a plateau value at ~2.4 ns. We have also monitored the shape of the droplet, which also stabilizes within ~2.4 ns (the droplet contains only 4,000 water molecules, which has a much shorter relaxation time scale than a macroscopic droplet). The substrate is dragged toward the positive x direction with a constant velocity of 10 m/s. At the same time, the x-position of center of mass (COM) of the water droplet is held fixed. Moreover, the velocity of COM along the x direction is held at zero. This simulation setup leads to a moving water droplet sliding on a substrate such that both the advancing and receding angles can be measured in the same molecular simulation. After the droplet reaches the steady shape, we acquire data using the next 2.4 ns while the temperature is maintained at 298 K. We generated the equimolar contour of the droplet based on its time-averaged shape. The advancing and receding angles were then obtained by fitting the partial contours 10–20 Å away from the substrate. This simulation methodology enables measurement of the dynamic contact angles in MD simulations. To our best
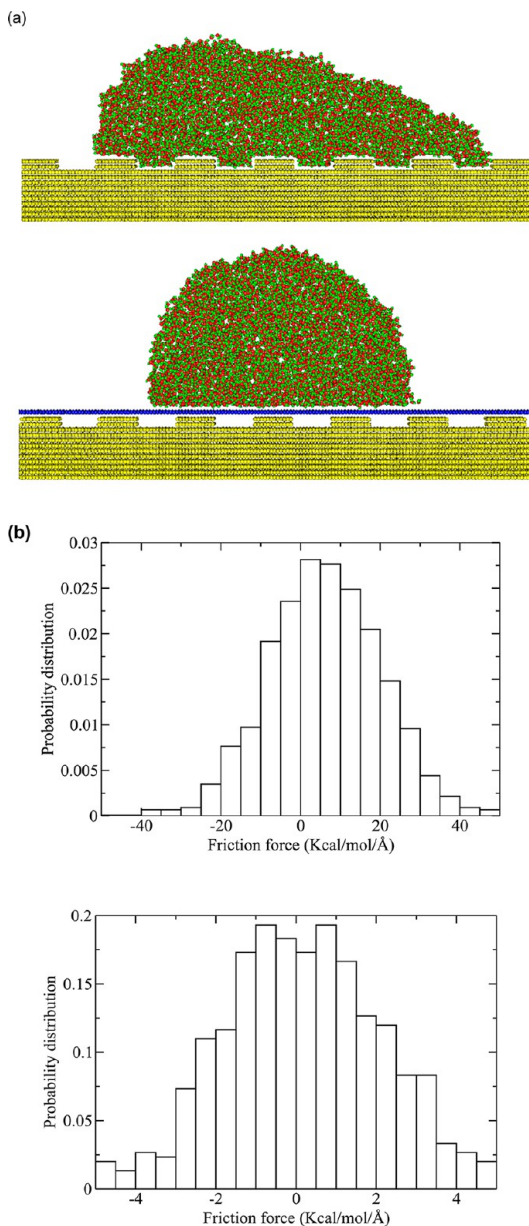
Figure 5. Molecular dynamics (MD) simulations. (a) A snapshot of a moving water droplet (the substrate is moving to the right) on a rough nanotextured Cu surface without a graphene drape (upper graph) and with a monolayer graphene drape (lower graph) during our molecular dynamics simulations. The porosity of the surface (projected area of the solid–liquid contacts divided by the total projected area of the droplet) is ~0.5 which is similar to the experiments. **(b)** The friction force distribution for water droplet on bare patterned copper (upper graph) and graphene-coated patterned copper (lower graph).

knowledge, this is the only strategy that can provide a steady-state measurement for both the advancing and the receding angles in MD simulations.

As shown in Figure 5a, the shape of the moving water droplet (the substrate is moving to the right) on the roughened Cu surface is significantly altered by the monolayer graphene drape. The simulations indicate that the moving water droplet fully wets the undraped (rough) Cu surface reaching the Wenzel state, which is

consistent with experimental observations. However, once it is draped by single-layer graphene, there is no indication of water penetrating into the surface. For the undraped (rough) Cu surface, the advancing angle (84°) is very different from the receding angle (39°). However, for Cu with graphene-draping, the advancing and receding angles are both close to ~103°. Note that the MD simulations assume a perfectly flat (smooth) and defect-free graphene surface which leads to almost zero hysteresis. In the experiments, the hysteresis is larger because the graphene sheet is wrinkled (due to the transfer) and rough since it conforms to the topology of the sharp Cu nanorod tips. Wetting hysteresis can be correlated to the frictional force between the water droplet and the substrate. As shown in Figure 5b, the friction force (from the simulations) for water on the bare (*i.e.*, roughened) Cu surface is ~5 kcal/mol/Å, while the friction force on the same surface after it has been draped by graphene is almost negligible. This observation agrees very well with our drop impact experiments (see Figure 4) which indicated that the energy dissipation in the nanotextured rough surface (high friction) is up to an order of magnitude higher as compared to the corresponding graphene-draped surface (low friction).

CONCLUSIONS

The main obstacle to the motion of water drops on a solid surface arises from contact angle hysteresis that pins the drop edge. This is especially true for textured (or rough) surfaces where suspended water droplets can readily penetrate into the surface roughness features and get pinned to the substrate. We show in this work that a minimally invasive (monolayer) graphene drape placed over a nanotextured rough surface prevents the pinning of the contact line and significantly reduces the contact angle hysteresis. Increasing the number of graphene layers in the drape further reduces the contact angle hysteresis. Molecular dynamics simulations confirm that penetration of water into the surface roughness features is blocked by the graphene drape leading to a dramatic reduction in energy dissipation at the droplet−substrate interface. Graphene drapes could therefore enable enhanced droplet mobility which is required in a variety of applications in microfluidics and nanofluidics.

One of the key issues that warrants further investigation is whether or not superhydrophobicity (water contact angle > 150°) can be maintained on a graphene-draped surface. Our results and the results in ref 24 indicate that the maximum water contact angle that can be achieved on a graphene draped surface is ~96°. However this is the case when the graphene sheet remains flat on the surface roughness features, which will happen if the spacing between the roughness features is of the order of tens of nanometers as in our case and also for the surface in ref 24. However consider a situation in which the spacing between the roughness features is of the order of micrometers (Figure S1 in the Supporting Information). In such a situation the highly flexible graphene drape could partially droop or sag into the roughness features and consequently one would expect an air gap to be maintained between the water contact line and the graphene drape. The water contact angle in such a situation could indeed be superhydrophobic and merits further investigation. For such a surface, we expect that impacting water drops will be unable to penetrate into the cavities between the microscale roughness features due to the impermeable graphene drape enabling the drop to remain in the Cassie state.

Graphene drapes could also open new vistas in the field of electro-wetting on rough surfaces. Electro-wetting is typically performed on hydrophobic surfaces but contact line pinning and Cassie-to-Wenzel state transition is a major impediment to reversible electro-wetting on textured (rough) surfaces. A graphene drape coated with a dielectric coating material (Figure S2 in Supporting Information) may drastically reduce contact line pinning and enable reversible electro-wetting which is an enormous challenge on rough surfaces.

MATERIALS AND METHODS

Copper Nanorod Deposition. Copper nanorods were deposited using DC magnetron sputtering with an oblique angle flux incidence of ~85° with respect to the surface normal. The copper target was obtained from Plasmaterials, Inc. with a purity of 99.999%. To deposit vertically aligned copper nanorods, the substrate was mounted on a stepper motor and rotated at a speed of 30 rpm. Vertically aligned nanorods however show a significant fanning out of the structures which drastically reduces the porosity of the film. To reduce fanning out, the substrate rotation direction was changed periodically from clockwise to counter-clockwise and vice versa. Depositions were carried out at room temperature. A presputtering stage in which the substrate was shielded from the flux by a manually controlled shutter was employed to remove possible contaminants from the copper target prior to the final deposition step.

The deposition parameters used were chamber base pressure of ~8 × 10⁻⁷ Torr, power of 200 W, an ultrapure Ar working pressure of ~2.5 mTorr, and Ar flow rate of 2.01 sccm.

Graphene Synthesis. Single layer graphene was grown using chemical vapor deposition on ~25 μm thick copper foils;[22] the growth procedure used was an optimized version developed for our specific furnace. An alumina boat was loaded with a 2 cm × 2 cm copper foil which was placed in a 3 zone split tube furnace and pumped down to 2 mTorr and then purged with argon twice. Hydrogen was set to a flow rate of 8 sccm which corresponds to a pressure of 120 mTorr. The furnace was then ramped to 1020 °C in 30 min and the copper foils were then annealed at this temperature for 30 min. The graphene growth was initiated by turning on the methane (flow rate = 120 sccm) and this drove the pressure up to 1.2 Torr. After 20 min of graphene growth the furnace heaters were turned off and the

lid was opened to cool the tube rapidly without turning off the flow of gases. After the tube cooled to ~400 °C the flowing hydrogen and methane was replaced by argon to purge the system till the sample temperature was reduced to the ambient.

Graphene Transfer onto the Cu Nanorods. PMMA (dissolved in chlorobenzene @ 50 mg/mL) was spin coated onto one side of the copper foil with graphene. The other side was etched with oxygen plasma to remove the graphene. The copper foil/graphene/PMMA stack was gently placed with the exposed copper side floating onto a solution of 0.25 M ammonium persulfate (APS) to etch the copper. After 12 h the graphene/PMMA stack was transferred to a fresh bath of 0.5 M ammonium persulfate (APS) to ensure that the copper was completely etched. This graphene/PMMA stack was transferred to DI water and washed gently by transferring it repeatedly into pure DI water baths. The graphene/PMMA stack was finally transferred onto the Cu nanorod surface gently to ensure no tearing of the graphene/PMMA stack and was dried in air; this allows the water to slowly evaporate without rupturing the graphene/PMMA stack.[27] Next the Cu nanorod with graphene/PMMA was heated in an oven gradually to ~100 °C for 15 min to allow the PMMA to partially flow; this in turn enables the graphene sheet to attach itself to the Cu nanorods surface. This step proved to be critical as rapid heating damaged the graphene/PMMA stack while heating above 100 °C fused the Cu nanorods and completely modified the original surface. The Cu nanorod sample with graphene/PMMA was then gently dipped into acetone at 50 °C for 15 min to strip away the PMMA layer followed by dipping in ethanol to rinse any residue. The final step was air drying of the Cu nanorods surface draped with graphene.

Raman Spectroscopy. The Raman spectrum for the sample was measured using a Renishaw Raman Scope 2000 which was equipped with 514 nm green laser and a 50× microscope objective lens. CVD grown graphene, from the same batch used for the "graphene drape", was transferred onto a silicon wafer with a 285 nm thick SiO_2 layer to allow easy location and measurement of the Raman signal.

Contact Angle Measurements. Static contact angle measurements as well as advancing and receding contact angle measurements were performed on a 500-F4 Ramé Hart goniometer. Images captured on the goniometer were analyzed using Low-Bond Axisymmetric Drop Shape Analysis (LB-ADSA) plugin on ImageJ software. For the droplet impact study, images were captured using a high-speed PhantomV4 camera at 800 frames per second with an exposure time of 80 μs. Extremely low contact angles during the pancake phase had to be measured manually since the LB-ADSA plugin did not work at those values. An average value of the left and right side contact angles was taken in those cases.

Conflict of Interest: The authors declare no competing financial interest.

Supporting Information Available: Videos showing the impact of water droplets on the undraped Cu nanorods surface and the graphene draped Cu nanorods surface; concept schematics showing possible engineering applications of graphene-based drapes. This material is available free of charge *via* the Internet at http://pubs.acs.org.

REFERENCES AND NOTES

1. Mugele, F. Fundamental Challenges in Electrowetting: From Equilibrium Shapes to Contact Angle Saturation and Drop Dynamics. *Soft Matter* **2009**, *5*, 3377–3384.
2. Lau, K. K.; Bico, J.; Teo, K. B.; Chhowalla, M.; Amaratunga, G. A.; Milne, W. I.; McKinley, G. H.; Gleason, K. K. Superhydrophobic Carbon Nanotube Forests. *Nano Lett.* **2003**, *3*, 1701–1705.
3. Chen, X.; Wu, J.; Ma, R.; Hua, M.; Koratkar, N.; Yao, S.; Wang, Z. Nanograssed Micropyramidal Architectures for Continuous Dropwise Condensation. *Adv. Funct. Mater.* **2011**, *21*, 4617–4623.
4. Blossey, R. Self-Cleaning Surfaces-Virtual Realities. *Nat. Mater.* **2002**, *2*, 301–306.
5. de Ruiter, J.; Oh, J. M.; van den Ende, D.; Mugele, F. Dynamics of Collapse of Air Films in Drop Impact. *Phys. Rev. Lett.* **2012**, *108*, 074505.
6. Shastry, A.; Marianne, J.; Böhringer, K. F. Directing Droplets Using Microstructured Surfaces. *Langmuir* **2006**, *22*, 6161–6167.
7. Zhu, J.; Andres, C. M.; Xu, J.; Ramamoorthy, A.; Tsotsis, T.; Kotov, N. A. Pseudonegative Thermal Expansion and the State of Water in Graphene Oxide Layered Assemblies. *ACS Nano* **2012**, *6*, 8357–8365.
8. Lafuma, A.; Quere, D. Superhydrophobic States. *Nat. Mater.* **2003**, *2*, 457–460.
9. Miwa, M.; Nakajima, A.; Fujishima, A.; Hashimoto, K.; Watanabe, T. Effects of the Surface Roughness on Sliding Angles of Water Droplets on Superhydrophobic Surfaces. *Langmuir* **2000**, *16*, 5754–5760.
10. Singh, E.; Chen, Z.; Houshmand, F.; Ren, W.; Peles, Y.; Cheng, H.-M.; Koratkar, N. Superhydrophobic Graphene Foams. *Small* **2013**, *9*, 75–80.
11. Jisr, R. M.; Rmaile, H. H.; Schlenoff, J. B. Hydrophobic and Ultrahydrophobic Multilayer Thin Films from Perfluorinated Polyelectrolytes. *Angew. Chem., Int. Ed.* **2004**, *44*, 782–785.
12. Martines, E.; Seunarine, K.; Morgan, H.; Gadegaard, N.; Wilkinson, C. D.; Riehle, M. O. Superhydrophobicity and Superhydrophilicity of Regular Nanopatterns. *Nano Lett.* **2005**, *5*, 2097–2103.
13. Nosonovsky, M.; Bhushan, B. Biomimetic Superhydrophobic Surfaces: Multiscale Approach. *Nano Lett.* **2007**, *7*, 2633–2637.
14. Acatay, K.; Simsek, E.; Yang, C.; Menceloglu, Y. Z. Tunable, Superhydrophobically Stable Polymeric Surfaces by Electrospinning. *Angew. Chem., Int. Ed.* **2004**, *43*, 5210–5213.
15. Shirtcliffe, N. J.; McHale, G.; Newton, M. I.; Chabrol, G.; Perry, C. C. Dual-Scale Roughness Produces Unusually Water-Repellent Surfaces. *Adv. Mater.* **2004**, *16*, 1929–1932.
16. Cassie, A. B. D.; Baxter, S. Wettability of Porous Surfaces. *T. Faraday Soc.* **1944**, *40*, 546–551.
17. Wenzel, R. N. Resistance of Solid Surfaces to Wetting by Water. *Ind. Eng. Chem.* **1936**, *28*, 988–994.
18. Krishnan, R.; Lu, T. M.; Koratkar, N. Functionally Strain-Graded Nanoscoops for High Power Li-Ion Battery Anodes. *Nano Lett.* **2011**, *11*, 377–384.
19. Li, C.; Wang, Z.; Wang, P.-I.; Peles, Y.; Koratkar, N.; Peterson, G. P. Nanostructured Copper Interfaces for Enhanced Boiling. *Small* **2008**, *4*, 1084–1088.
20. Schrader, M. E. Ultrahigh Vacuum Techniques in the Measurement of Contact Angles. III. Water on Copper and Silver. *J. Phys. Chem.* **1974**, *78*, 87–89.
21. Chen, S.; Brown, L.; Levendorf, M.; Cai, W.; Ju, S. Y.; Edgeworth, J.; Li, X.; Magnuson, C.; Velamakanni, A.; Piner, R. R.; et al. Oxidation Resistance of Graphene-coated Cu and Cu/Ni Alloy. *ACS Nano* **2011**, *5*, 1321–1327.
22. Li, X.; Cai, W.; An, J.; Kim, S.; Nah, J.; Yang, D.; Piner, R. R.; Velamakanni, A.; Jung, I.; Tutuc, E.; et al. Large-area Synthesis of High-Quality and Uniform Graphene Films on Copper Foils. *Science* **2009**, *324*, 1312–1314.
23. Rafiee, J.; Mi, X.; Gullapalli, H.; Thomas, A. V.; Yavari, F.; Shi, Y.; Ajayan, P. M.; Koratkar, N. A. Wetting Transparency of Graphene. *Nat. Mater.* **2012**, *11*, 217–222.
24. Shih, C. J.; Wang, Q. H.; Lin, S.; Park, K. C.; Jin, Z.; Strano, M. S.; Blankschtein, D. Breakdown in the Wetting Transparency of Graphene. *Phys. Rev. Lett.* **2012**, *109*, 176101.
25. Zheng, Q. S.; Yu, Y.; Zhao, Z. H. Effects of Hydraulic Pressure on the Stability and Transition of Wetting Modes of Superhydrophobic Surfaces. *Langmuir* **2005**, *21*, 12207–12212.
26. Bunch, J. S.; Verbridge, S. S.; Alden, J. S.; Van Der Zande, A. M.; Parpia, J. M.; Craighead, H. G.; McEuen, P. L. Impermeable Atomic Membranes from Graphene Sheets. *Nano Lett.* **2008**, *8*, 2458–2462.

27. Liang, X.; Sperling, B. A.; Calizo, I.; Cheng, G.; Hacker, C. A.; Zhang, Q.; Obeng, Y.; Yan, K.; Peng, H.; Li, Q.; *et al.* Towards Clean and Crack-Less Transfer of Graphene. *ACS Nano* **2011**, *5*, 9144–9153.

28. Werder, T.; Walther, J. H.; Jaffe, R. L.; Halicioglu, T.; Koumoutsakos, P. On the Water-Carbon Interaction for Use in Molecular Dynamics Simulations of Graphite and Carbon Nanotubes. *J. Phys. Chem. B* **2003**, *107*, 1345–1352.

29. Berendsen, H. J. C.; Grigera, J. R.; Straatsma, T. P. The Missing Term in Effective Pair Potentials. *J. Phys. Chem.* **1987**, *91*, 6269–6271.